ACS OMEGA

http://pubs.acs.org/journal/acsodf

Article

Enhanced Polymerization and Surface Hardness of Colloidal Siloxane Films via Electron Beam Irradiation

Junfei Ma, Ji-Hyeon Kim, Jaehun Na, Junki Min, Ga-Hyun Lee, Sungjin Jo,* and Chang Su Kim*

Cite This: *ACS Omega* 2021, 6, 13384−13390

Read Online

ACCESS | Metrics & More | Article Recommendations

ABSTRACT: Electron beam (EB) curing is a foldable hard coating process and has attracted significant research attention in the field of flexible electronic devices. In this study, we report a method for enhancing material surface hardness with low-energy EB curing in a short time. The low-energy EB improved the coating hardness of films by inducing cross-linking polymerization of the silicon-containing monomer. The hardness of the cured coating layer was measured as 3 H using a pencil hardness tester, and the transparency of the coating was higher than 90%. Owing to a series of cross-linking reactions between Si−O−C and Si−OH groups under EB curing and the formation of Si−Si bonds, the cured layer exhibited remarkable durability in the 100000-flexible cycle test. Additionally, the natural oxidation of the C−O groups on the surface of the coating formed carboxyl groups that improved the hydrophilic properties of the coating layer. To the best of our knowledge, this is the first study to propose that the hardness of polyethylene terephthalate films can be improved using low-energy EBs to rapidly cure silicon-containing coatings. Our results provide a novel and commercially viable approach for improving the hardness of touch screens and foldable displays.

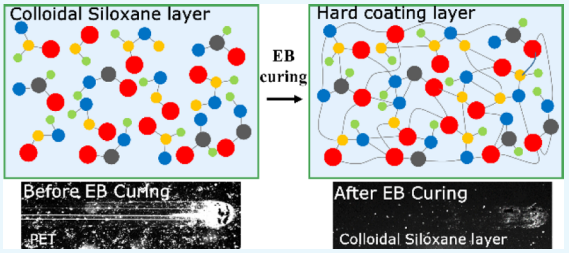

1. INTRODUCTION

Hard coating materials have attracted significant attention, owing to recent applications in foldable displays, touch panels, and smart windows. Hard coating layers are prepared from organic−inorganic hybrid materials based on colloidal siloxane nanoparticles using the sol−gel method.[1,2] To replace conventional thin glasses in applications, hard coating layers need to have a high light transmittance, low yellow index, high flexibility, and excellent mechanical properties (high hardness and scratch resistance). Although polyimide, polymethyl methacrylate, and polyethylene terephthalate (PET) films exhibit good folding resistance and low surface roughness, these single-structured organic substrates have inherent problems such as coloring, poor mechanical properties, poor ultraviolet (UV) transmission resistance, and low hardness that limit their applications in flexible electronic device coloring, poor mechanical properties, poor UV transmission resistance, and low hardness.[3,4] To overcome these drawbacks, organic−inorganic materials have been used to modify polymer surfaces via different curing methods, such as thermal curing,[5,6] UV curing,[7,8] and electron beam (EB) curing.[9] These curing methods enhance the hardness of coating materials, yielding better folding performance. Traditional thermal curing increases the hardness by changing the distribution of Si−O and Si−H bonds via chemical changes in the material.[10] However, long curing times, high energy consumption, complicated processes, and insufficient heat penetration depths restrict the application of thermal curing for hard coating. UV curing induces chemical and structural changes in esters via excited photons. During UV curing, photons induce photoinitiator separation into free radicals or cations, which combines monomers and oligomers in materials to polymers. However, UV curing requires a photoinitiator to effectively induce oligomer or single-molecule polymerization. Therefore, UV curing is limited by various properties of the photoinitiators, such as the reaction rate of the radicals and yellow index. Moreover, the hardness of the coating layer often depends on the type and amount of the photoinitiators used.[11] This reduces the controllability of the experimental procedure.

Owing to its low energy consumption, environmental friendliness, easy control, and rapid curing characteristics, EB is used in various curing processes, such as composite fabrication, hydrogel synthesis, wood product processing, antibacterial modification, electrode manufacture, and surface modification.[12−20] EB curing generates free radicals to induce polymerization in monomers, as in UV curing.[21] In contrast to UV curing, EB curing does not require the doping of specific photoinitiators and directly initiates the connection reaction

Received: March 17, 2021
Accepted: April 28, 2021
Published: May 11, 2021

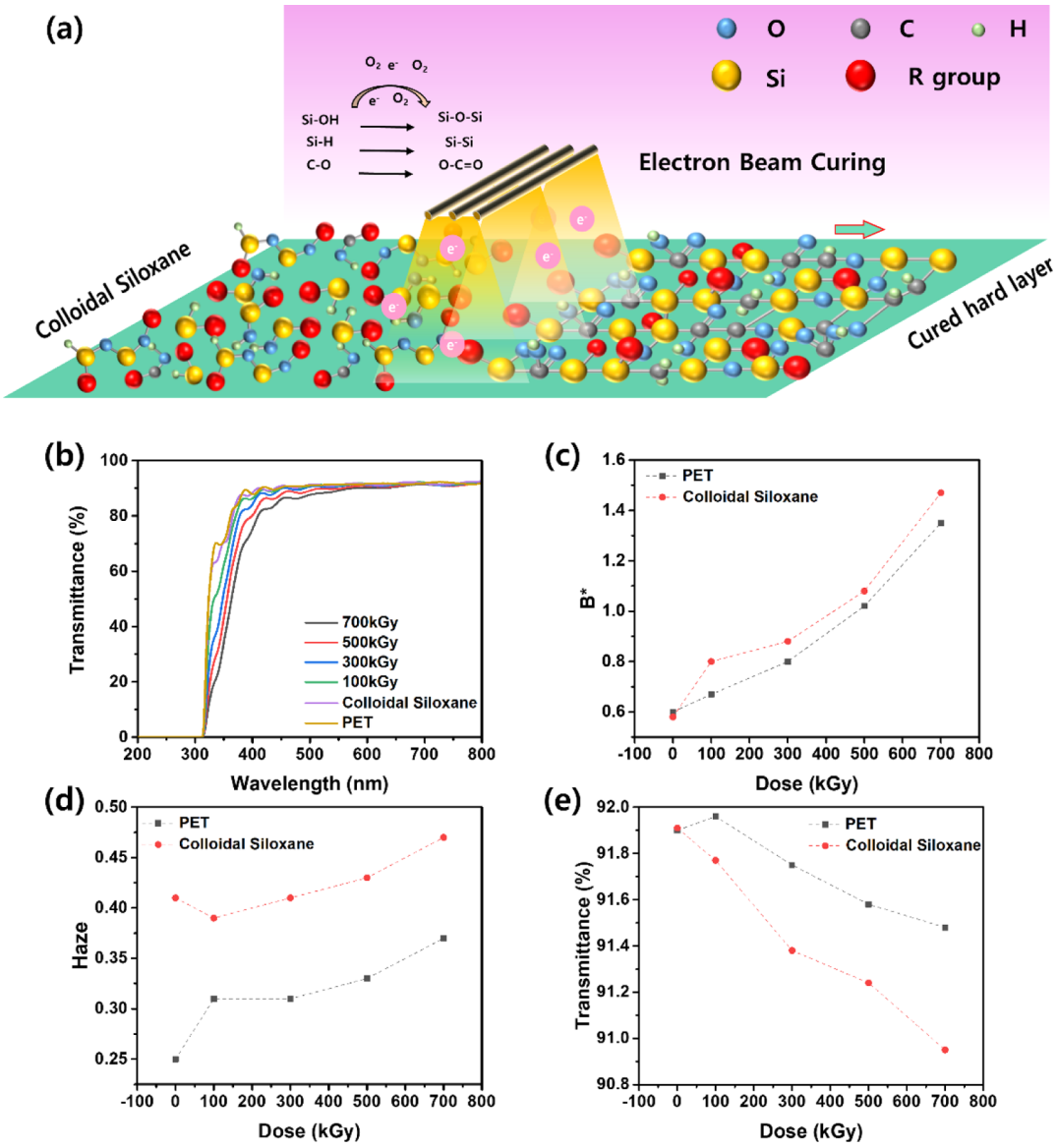

Figure 1. (a) Schematic diagram showing the reaction process of colloidal silica in EB curing. Schematic of the relationship between the optical characteristics and EB dose. (b) UV−visible (c) B^*, (d) haze, and (e) transmittance.

between the active parts.[22] It is well known that the increase in the surface hardness of cured materials is mainly due to the formation and enrichment of Si−O−Si bonds. Previous studies have confirmed that the Si−O−Si bond easily migrates to the coating surface during the curing process to form a dense Si−O−Si network structure, which gives the film surface excellent mechanical properties.[23] EB is also advantageous in that it does not produce volatile organic compounds harmful to the environment during curing. Moreover, recent studies have shown that EB curing is more effective than UV curing in enhancing the surface hardness of materials.[24]

Inspired by these motivations, we characterize a colloidal siloxane solution coated on a PET substrate cured by EB curing with different doses in this study. Since the EB dosage serves as the only factor affecting the hardness of the cured coating layer, the operability and controllability of the experiment were simplified and improved. The cured colloidal siloxane films exhibited outstanding foldability, high transparency, and good hardness. Since the low-energy electrons excited by the EB can directly excite the reaction sites of the multifunctional monomers, such as the bonds between oligomers and monomers, the hardness of the coating layer is improved significantly.

2. RESULTS AND DISCUSSION

2.1. Optical Properties of the Coating Layer. Figure 1a shows a schematic diagram of the EB curing of a colloidal siloxane layer. The Si−H, Si−OH, and C−O bonds undergo polymerization and oxidation under the combined action of low-energy electrons and oxygen. To analyze the optical influence of the PET substrate on colloidal siloxane after EB curing, we measured the transmittance of various samples coated on the PET substrate in the visible range, and the results are shown in Figure 1b. The wavelength range of the UV−visible spectrometer (Agilent, Cary 5000, USA) was set to 200 to 800 nm. The transmittance of the film exhibits a significant drop in the 320 and 550 nm regions, which is mainly due to the strong UV absorption of the colloidal siloxane layer. In the wavelength range of 550−800 nm, the transparency of various samples was stable at 90%. The change

https://doi.org/10.1021/acsomega.1c01429
ACS Omega 2021, 6, 13384−13390

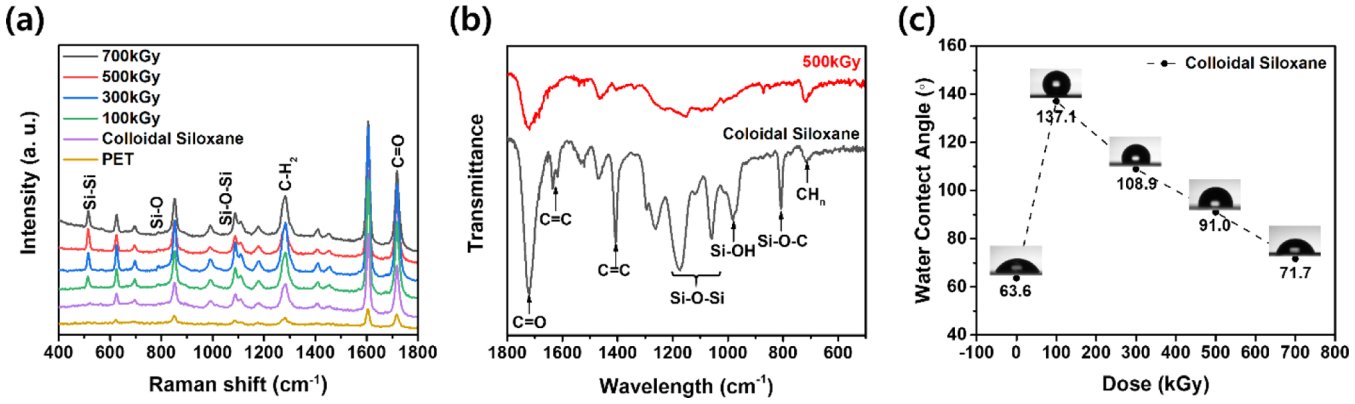

Figure 2. (a) Raman spectra of PET (in brown) and colloidal siloxane cured with different doses: 0 kGy (in purple) 100 kGy (in green), 300 kGy (in blue), 500 kGy (in red), and 700 kGy (in black). (b) FT-IR spectra of colloidal siloxane before (black) and after (red) EB curing at a dose of 500 kGy. (c) Water contact angle measurements of the colloidal siloxane layer with different doses.

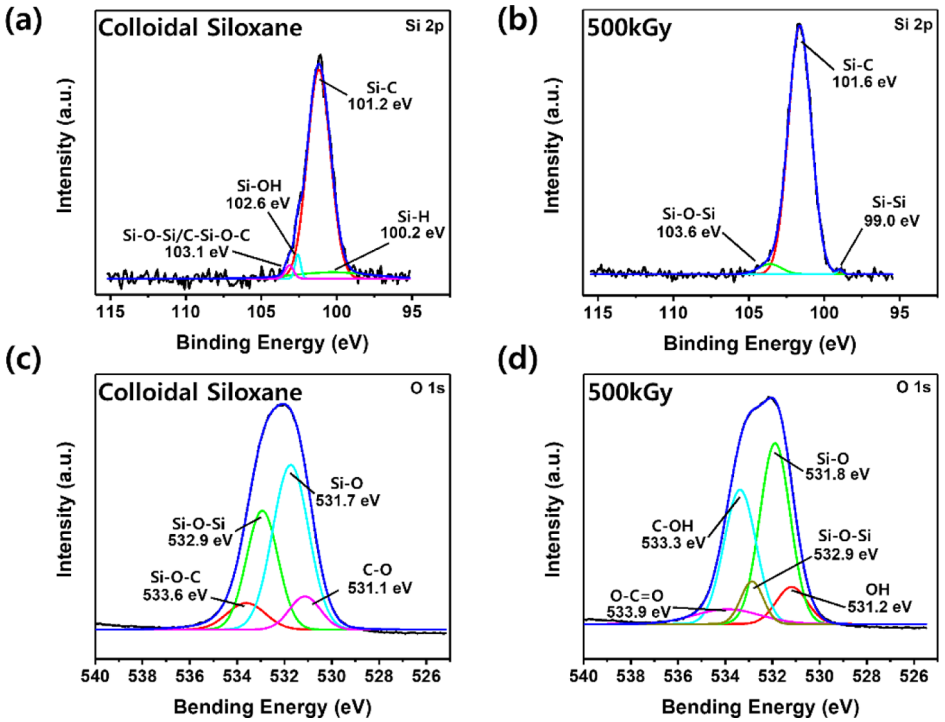

Figure 3. (a) XPS Si 2p spectra of the colloidal siloxane coating layer (a) before and (b) after EB curing with 500 kGy. The O 1s spectra show the peak positions of colloidal siloxane coating layer (c) before and (d) after EB curing with 500 kGy.

curve of the yellowness (B^*), haze, and transmittance of the colloidal siloxane layer after curing was investigated using a haze meter (COH 400, Nippon Denshoku Co., Ltd., Japan), as shown in Figure 1c,d, and e respectively. EB irradiation causes the PET film to undergo thermal aging.[25] The optical performance decreased more significantly with an increase in the EB dosage. Although the trend in the optical properties of the colloidal silica coating on PET was negatively affected by the EB, the trend of the change was positively correlated with the optical change curve of PET. Therefore, it is inferred that the decrease in the optical properties of colloidal silica is mainly due to the yellowing of the PET substrate.

2.2. Fourier Transform Infrared and Raman Spectra. To further confirm the presence of PET and the coating layer under different conditions, we investigated the samples using a Raman spectrometer (NS 200; Daejeon, Korea). As shown in Figure 2a, the cross-linking reaction between the colloidal siloxane was obtained by measuring the change in the strength of the Si−Si bond after curing, using a high-resolution Raman microscope. For the cured coating layer, the peak at 520 cm^{-1} is due to the Si−Si bond produced by the curing process.[26,27] The other characteristic peaks are due to Si−O−Si bending (1000−1200 cm^{-1}), CH_2 bending (1290 cm^{-1}), and C═O stretching (between 1700 and 1750 cm^{-1}).[28,29]

Fourier transform infrared (FT-IR) spectroscopy (Nicolet iS50, Thermo Fisher co., Korea) was used to investigate the desired functional groups in the cured coating layer. The water contact angle of the colloidal siloxane/PET film after curing with different doses of EB measured using a contact angle meter (Smart Drop Lab, Korea) is shown in Figure 2c. The size of the contact angle increased from 63.3 to 137.1° with an increase in the excited EB dose from 0 to 100 kGy. Since the colloidal siloxane coatings contain a large amount of hydrophilic solvent, they exhibit better hydrophilicity than

https://doi.org/10.1021/acsomega.1c01429
ACS Omega 2021, 6, 13384−13390

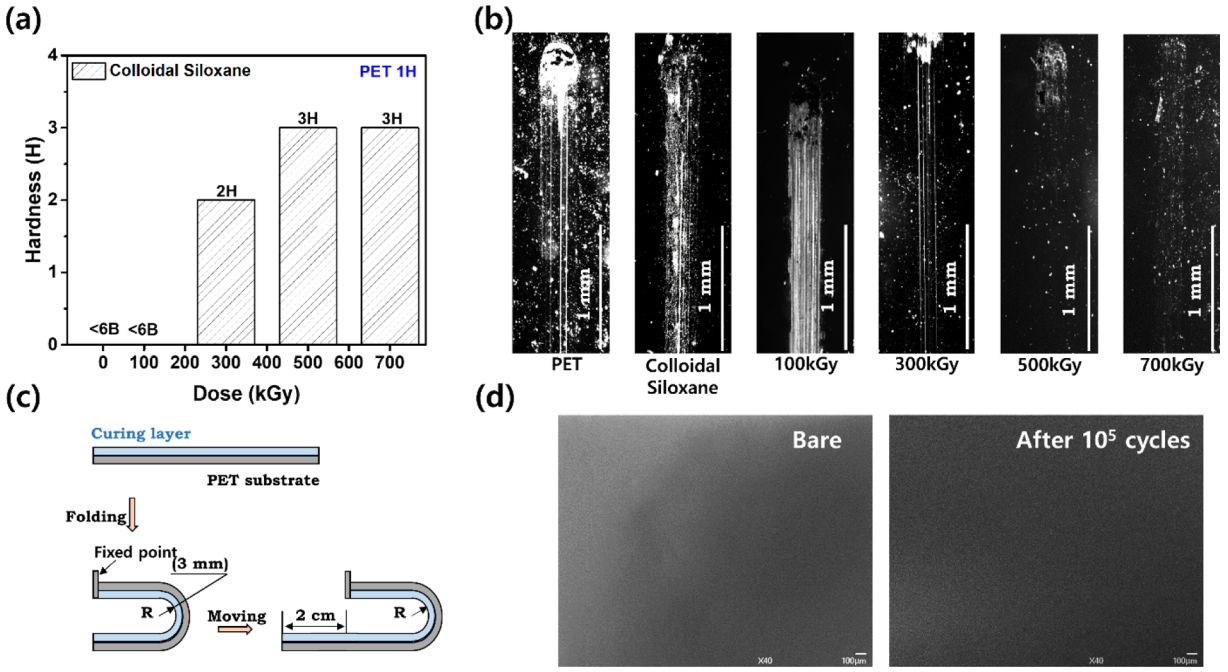

Figure 4. (a) Hardness of the PET and colloidal siloxane layers at EB doses of 0, 100, 300, 500, and 700 kGy. Micrograph of a typical failure pattern of (b) PET film and coated colloidal siloxane substrate with different doses after a pencil hardness test of 3 H. The scale bar is 1 mm. (c) Schematic of digital pictures of EB-cured colloidal siloxane with 500 kGy doses. (d) Bare colloidal siloxane coating layer (left) and after bending test after 10^5 cycles (right). The scale bar is 100 μm.

PET substrates. When the dosage of EB was increased to 100 kGy, the aqueous solvent in the colloid volatilized. In the process of increasing the EB dose from 100 to 700 kGy, the combined effect of EB and oxygen oxidized the C−O bond into a hydrophilic carboxyl group generated on the surface of the hard coating. This increased the wettability of the coating surface.[30−32] Figure 2b shows the FT-IR spectra of the colloidal siloxane and colloidal siloxane layers cured by EB at a dose of 500 kGy. The following peaks were observed: the peak at approximately 1730 cm^{-1} was derived from the C═O group,[33] and the peaks at 1640 and 1400 cm^{-1} were due to C═C stretching.[34,35] The intensity of the C═C peak was reduced significantly after EB curing, owing to oxidation. In addition, the Si−O−Si peak (1000−1200 cm^{-1}), Si−OH peak (880−980 cm^{-1}),[36] Si−O−C peak (700−950 cm^{-1}),[37] and CH_n peak (740 cm^{-1}) are also marked. The Si−O−C and Si−OH peaks are converted into Si−Si and Si−O−Si bonds, respectively. Thus, the intensity of these peaks weakened after the curing process.

2.3. X-Ray Photoelectron Spectroscopy Analysis. The O 1s spectrum shown in Figure 3 shows four peaks: Si−H (100.2 eV), C−Si (101.2 eV), Si−OH (102.6 eV), Si−O−Si, or C−Si−O−C (103.1 eV).[38−41] However, only three peaks are observed in the X-ray photoelectron spectroscopy (XPS) (K-alpha, Thermo Fisher co., Waltham, USA) results of the coating after EB curing in Figure 3b, corresponding to the Si−Si bond (99.0 eV),[42] Si−C bond (101.6 eV), and Si−O−Si bond (103.6 eV). The OH and Si−H bonds disappear with the formation of Si−Si bonds because the EB breaks the Si−H bonds and converts them into free radical states. The suspended silicon atoms then recombine into Si−Si bonds.[43−45] The other change in the silicon-containing functional groups after EB curing is the change in the Si−OH bonds to Si−O−Si bonds.[10] Moreover, it can be seen in Figure 3c,d that the EB-cured colloidal siloxane coating layer further affects carbon-containing groups. Figure 3c shows that the O 1s regions in the XPS spectra of colloidal siloxane can be divided into four peaks at 531.1, 531.7, 532.9, and 533.6 eV. These can be attributed to C−O, Si−O, Si−O−Si, and Si−O−C, respectively.[46−49] By contrast, the O1s peak of the EB-cured sample in Figure 3d exhibits the following five peaks: OH (531.2 eV),[50] Si−O−Si (532.9 eV), Si−O (531.8 eV), C−OH (533.3 eV),[51] and O−C═O (533.9 eV).[52] It is worth noting that the surface of the EB-cured sample lacks Si−O−C bonds. Moreover, the peaks of the carboxyl functional groups and hydrogen−oxygen bonds increased. The formation of the carboxyl groups is mainly due to the combination of free radicals and oxygen under the action of EBs to assist the oxidation of C−O bonds in siloxane.[30]

2.4. Hardness Testing. Scratch resistance is an important evaluation index for measuring the surface performance of hardness coatings, and it determines the suitability of the materials for various applications. To estimate the hardness of the cured colloidal siloxane layers after EB curing, the cured layers were measured using a pencil hardness tester (TO-540, TESTONE Co., Ltd., Korea). The pencil was fixed above the sample, and the angle between the pencil and the sample was set to 45 °C. A test load of 1 kg was automatically pushed five times in different areas on the sample for hardness evaluation. Figure 4a shows that the hardness of colloidal siloxane-500 kGy reached the maximum value (3 H). By comparison, the bare PET film exhibited a hardness of 1 H. These results can be attributed to the cross-linking of the colloidal siloxane monomers and oligomers during EB curing. Particularly, this observation is due to the fact that the layer was not EB-cured, and the EB dosage was 100 kGy. The degree of curing of the coating is related to the EB dosage. When the EB dose was further increased to 700 kGy, the hardness of the colloidal siloxane coating was maintained at 3 H. This may be because the thickness of the coating limits the hardness from increasing

https://doi.org/10.1021/acsomega.1c01429
ACS Omega 2021, 6, 13384−13390

further. Figure 4b (from left to right) shows the scratches on PET and the colloidal siloxane layer after curing with different doses of EB under an optical magnifier (Thermo Fisher Scientific Co., Ltd., Korea). It can be seen that the scratches reduce gradually as the EB dose increases during the curing process. After the EB dose increased from 500 to 700 kGy, the surface of the hard coating treated by the EB did not contain any scratches. In particular, the colloidal siloxane layers irradiated at 500 and 700 kGy maintained the integrity of the surface structure of the coating layer after undergoing a scratch test. At the same time, the hardness of the coating no longer increased with an increase in the EB dose. This suggests that when the EB dose is low, the hardness of the coating mainly depends on the EB dose. However, when the EB dose is increased to 500 kGy, the increase in the hardness of the coating is mainly limited by the monomer or oligomer of the coating itself.

2.5. Bending Testing. Resistance to bending fatigue is also a common index for measuring the mechanical properties of hard coatings. Since the colloidal siloxane layer is cured with 500 kGy, it exhibits excellent mechanical and optical properties. Therefore, the EB-cured colloidal siloxane layer with 500 kGy (bare) doses was selected for comparison after the bending test with 10^5 cycles. The bending resistance of the hard coating layers for 10^5 cycles was investigated using a flexural endurance tester (CKMFET 1400M, CKSI Co., Ltd., Korea). A schematic of the U-shaped bending test of the sample is shown in Figure 4c. The bending radius of the EB-cured layer with a dosage of 500 kGy was set to 3 mm, and the horizontal reciprocating distance of the cam with 300 rpm rotation to the carrier was set to 2 cm. Figure 4d shows the scanning electron microscopy images of the (left) bare sample and (right) after 10^5 bending cycles. Compared with the bare sample, no creases or cracks were observed on the surface of the cured hard coating after 10^5 bending cycles, which demonstrated that the hard coating was not structurally damaged. This shows that the colloidal siloxane solution can be converted into a flexible transparent coating layer with exceptional mechanical properties through EB curing. Moreover, no wrinkles or delamination were observed in the crease area of the coating, which also indicated that the hard coating adhered well to the PET substrate.

3. CONCLUSIONS

We introduced a curing method to improve the surface hydrophobicity and hardness of flexible curved transparent coatings. We investigated the surface hardness, optical properties, chemical structure, and folding resistance of the coating layer after EB curing at different doses. The hardness of the EB-cured coating layer reached 3 H, and the transparency exceeded 90%. Furthermore, the bending resistance test of the cured coating layer reached 10^5 cycles. A bending radius of 3 mm exhibited good bending resistance. Since the per-cured coating solution is certain, the electrons excited by the low-energy EB with a dose of 500 kGy penetrate the material and convert the Si−OH and Si−O−C groups to Si−O−Si or Si−Si bonds, respectively. Rapid transformation of the material phase was realized while greatly increasing the hardness of the cured coating. In addition, EB-catalyzed grafting of the carboxyl group onto the coating surface enhances the hydrophilicity of the colloidal siloxane hard coating layer. The results reveal that the low-energy electrons excited by the EB contribute to the rapid curing of the coating. It also improves the mechanical properties by inducing crosslinking agents to promote the re-condensation of monomers and oligomers. Finally, it is worth noting that the oxidation induced by the low-energy EB in this experiment increased the hydrophilicity of the coating surface. Therefore, increasing the coating hardness while maintaining the hydrophobicity of the coating is a challenging task and an open scope for future work.

4. EXPERIMENTAL SECTION

4.1. Materials. The materials used in this experiment included 40% colloidal siloxane hybrid solution (colloidal siloxane), acetone, and isopropyl alcohol (IPA). Colloidal siloxane containing single molecules was provided by Korea Inno Tech (Changwon, Korea; 40 wt % solubility). The PET film was purchased from KIMOTO Co., Ltd. (Japan; 100 μm). The other reagents (acetone and IPA solution) maintained the original concentration and state.

4.2. Preparation of the Colloidal Siloxane Layer. The colloidal siloxane original ink was ultrasonicated for 5 min using an ultrasonic cleaner (SD 200H, Wankyung Tech, Korea) to obtain a homogeneous dispersion solution. Subsequently, the previously processed colloidal siloxane solution was coated on the PET substrate with a bar coater to fabricate a per-cured coating layer at room temperature (GBC-A4, GIST Co., Ltd., Korea). The colloidal siloxane coatings were dried at room temperature and passed through the EB emitting cavity at a rate of 3 m/min (EBlab-200, COMET, Switzerland), and the colloidal siloxane layer coated on the PET substrate was exposed to EB curing at 0, 100, 300, 500, and 700 kGy. The thickness of the coating was measured using a Bruker stylus profiler (DektakXT, Bruker Korea Co., Ltd.) with a thickness gauge of 3.7 μm.

4.3. Characterization. The optical properties of the hard coating layers were characterized using a color meter (Nipon Denshoku Industries Co., Saitama Japan) and a UV−Vis spectrometer (Cary 5000 UV−Vis−NIR, Agilent co., Santa Clara, CA, USA). The thickness of the coating layers was measured using a stylus profilometer (DektakXT, Bruker Co., Billerica, Germany), and the chemical state and surface morphology of the coating layers were characterized using XPS (K-alpha, Thermo Fisher co., Waltham, USA), high-resolution Raman spectroscopy (NS200, Nanoscope co., Deajeon, Korea), FT-IR spectroscopy (Nicolet iS50, Thermo Fisher co., Korea), and scanning electron microscopy (JSM-6700F, JEOL Co., Akishima, Japan). The hydrophilicity was measured using a contact angle analyzer (E-Flex Co., Bucheon, Korea). The hardness and surface scratches of the layers were measured using a motorized pencil hardness tester (CT-PC2, Korea) and an imaging system (EVOS M5000, Thermo Fisher co., Waltham, USA). The bending resistance of the coating layers was measured using a flexible tester (CKMFET 1400M, CKSI Co., Ltd., Korea).

AUTHOR INFORMATION

Corresponding Authors

Sungjin Jo − *School of Architectural, Civil, Environmental, and Energy Engineering, Kyungpook National University, Daegu 41566, South Korea;* orcid.org/0000-0001-6407-0233; Email: sungjin@knu.ac.kr

Chang Su Kim − *Department of Nano-Bio Convergence, Korea Institute of Materials Science (KIMS), Changwon 51508, South Korea;* orcid.org/0000-0003-3367-3087;

https://doi.org/10.1021/acsomega.1c01429
ACS Omega 2021, 6, 13384−13390

Phone: 82-55-2803696; Email: cskim1025@kims.re.kr; Fax: 82-55-280-3570

Authors

Junfei Ma − *Department of Nano-Bio Convergence, Korea Institute of Materials Science (KIMS), Changwon 51508, South Korea; School of Architectural, Civil, Environmental, and Energy Engineering, Kyungpook National University, Daegu 41566, South Korea;* orcid.org/0000-0003-4191-4936

Ji-Hyeon Kim − *Department of Nano-Bio Convergence, Korea Institute of Materials Science (KIMS), Changwon 51508, South Korea;* orcid.org/0000-0003-1780-0728

Jaehun Na − *Gimhae Industry Promotion & Bio-medical Foundation, Gimhae 50969, Gyeongnam, South Korea*

Junki Min − *Gimhae Industry Promotion & Bio-medical Foundation, Gimhae 50969, Gyeongnam, South Korea*

Ga-Hyun Lee − *Department of Nano-Bio Convergence, Korea Institute of Materials Science (KIMS), Changwon 51508, South Korea; School of Architectural, Civil, Environmental, and Energy Engineering, Kyungpook National University, Daegu 41566, South Korea*

Complete contact information is available at: https://pubs.acs.org/10.1021/acsomega.1c01429

Author Contributions

J.M. designed the study, analyzed the data, and wrote the manuscript. J.-H.K. participated in the analysis of the data and a certain degree of grammar editing of the article. J.N. and J.M. participated in the electron beam curing coating experiment. G.-H.L. assisted in the design and operation of this experiment. C.S.K. and S.J. provided the experimental materials and guided the experimental design plan.

Notes

The authors declare no competing financial interest.

■ ACKNOWLEDGMENTS

This research was supported by the "Nano-Product Upgrading Program using Electron Beam" through the Gyeongnam-do & Gimhae and the Technology Development Program (S2830309) funded by the Ministry of SMEs and Startups (MSS, Korea) and the fundamental research program (PNK7400) of the Korea Institute of Materials Science.

■ REFERENCES

(1) Li, G.; Wang, L.; Ni, H.; Pitman, C. N., Jr Polyhedral Oligomeric Silsesquioxane (POSS) Polymers and Copolymers: A Review. *J. Inorg. Organomet. Polym.* **2001**, *11*, 123−154.

(2) Phillips, S. H.; Haddad, T. S.; Tomczak, S. J. Developments in nanoscience: polyhedral oligomeric silsesquioxane (POSS)-polymers. *Curr. Opin. Solid State Mater. Sci.* **2004**, *8*, 21−29.

(3) Kang, T.; Tang, L.; Qu, J. Preparation and Properties of High Hardness Ultraviolet Curable Polyethylene Terephthalates Surface Coatings Modified with Octavinyl-Polyhedral Oligomeric Silsesquioxane. *Coatings* **2018**, *8*, 411.

(4) Wang, W.; Liang, T.; Zhang, B.; Bai, H.; Ma, P.; Dong, W. Green functionalization of cellulose nanocrystals for application in reinforced poly(methyl methacrylate) nanocomposites. *Carbohydr. Polym.* **2018**, *202*, 591−599.

(5) Chirachanchai, S.; Yoswathananont, N.; Laobuthee, A.; Ishida, H. Silica surface modified with benzoxazine-functional silane. *Compos. Interfaces* **2001**, *8*, 355−366.

(6) Guo, K.; Li, P.; Zhu, Y.; Wang, F.; Qi, H. Thermal curing and degradation behaviour of silicon-containing arylacetylene resins. *Polym. Degrad. Stab.* **2016**, *131*, 98−105.

(7) Jeon, S. J.; Lee, J. J.; Kim, W.; Chang, T. S.; Koo, S. M. Hard coating films based on organosilane-modified boehmite nanoparticles under UV/thermal dual curing. *Thin Solid Films* **2008**, *516*, 3904−3909.

(8) Yang, X.; Liu, J.; Wu, Y.; Liu, J.; Cheng, F.; Jiao, X.; Lai, G. Fabrication of UV-curable solvent-free epoxy modified silicone resin coating with high transparency and low volume shrinkage. *Prog. Org. Coat.* **2019**, *129*, 96−100.

(9) Kumar, V.; Misra, N.; Paul, J.; Bhardwaj, Y. K.; Goel, N. K.; Francis, S.; Sarma, K. S. S.; Varshney, L. Organic/inorganic nanocomposite coating of bisphenol A diglycidyl ether diacrylate containing silica nanoparticles via electron beam curing process. *Prog. Org. Coat.* **2013**, *76*, 1119−1126.

(10) Kim, D.-G.; Jung, B.; Kim, K. H.; Cho, K. Y.; Jeong, Y. C. Highly robust and transparent flexible cover window films based on UV-curable polysilsesquioxane nano sol. *J. Appl. Polym. Sci.* **2020**, *137*, 49012.

(11) Siew, Y. K.; Sarkar, G.; Hu, X.; Hui, J.; See, A.; Chua, C. T. Thermal Curing of Hydrogen Silsesquioxane. *J. Electrochem. Soc.* **2000**, *147*, 335.

(12) Abliz, D.; Duan, Y.; Zhao, X.; Li, D. Low-energy electron beam cured tape placement for out-of-autoclave fabrication of advanced polymer composites. *Composites, Part A* **2014**, *65*, 73−82.

(13) Cai, X.; Blanchet, P. Electron-Beam Curing of Acrylate/Nanoparticle Impregnated Wood Products. *Bioresources* **2015**, *10*, 3852−3864.

(14) Du, Z.; Janke, C. J.; Li, J.; Wood, D. L. High-Speed electron beam curing of thick electrode for high energy density Li-ion batteries. *Green Energy Environ.* **2019**, *4*, 375−381.

(15) Glass, S.; Kühnert, M.; Abel, B.; Schulze, A. Controlled Electron-Beam Synthesis of Transparent Hydrogels for Drug Delivery Applications. *Polymers* **2019**, *11*, 501.

(16) Stelescu, M.; Airinei, A.; Manaila, E.; Craciun, G.; Fifere, N.; Varganici, C.; Pamfil, D.; Doroftei, F. Effects of Electron Beam Irradiation on the Mechanical, Thermal, and Surface Properties of Some EPDM/Butyl Rubber Composites. *Polymers* **2018**, *10*, 1206.

(17) Trey, S. M.; Netrval, J.; Berglund, L.; Johansson, M. Electron-Beam-Initiated Polymerization of Poly(ethylene glycol)-Based Wood Impregnants. *ACS Appl. Mater. Interfaces* **2010**, *2*, 3352−3362.

(18) Zhang, J.; Duan, Y.; Ming, Y.; Wang, B. Investigation of irradiation dose rate on curing characteristics of carbon fiber/polymer composites by low-energy electron beam. *Polym. Adv. Technol.* **2019**, *30*, 179−186.

(19) Zhang, S.; Li, R.; Huang, D.; Ren, X.; Huang, T.-S. Antibacterial modification of PET with quaternary ammonium salt and silver particles via electron-beam irradiation. *Mater. Sci. Eng., C* **2018**, *85*, 123−129.

(20) Nik Salleh, N. G.; Firdaus Yhaya, M.; Hassan, A.; Abu Bakar, A.; Mokhtar, M. Effect of UV/EB radiation dosages on the properties of nanocomposite coatings. *Radiat. Phys. Chem.* **2011**, *80*, 136−141.

(21) Bouchakour, M.; Derouiche, Y.; Bouberka, Z.; Beyens, C.; Mechernène, L.; Riahi, F.; Maschke, U. Optical properties of electron beam- and UV-cured polypropyleneglycoldiacrylate/liquid crystal E7 systems. *Liq. Cryst.* **2015**, *42*, 1527−1536.

(22) Yao, B.; Zhao, H.; Wang, L.; Liu, Y.; Zheng, C.; Li, H.; Sun, C. Synthesis of acrylate-based UV/thermal dual-cure coatings for antifogging. *J. Coat. Technol. Res.* **2018**, *15*, 149−158.

(23) Mohamed, M.; Mohamed, H.; Moustafa, M.; Eid, A. A.; Mohamed, T. Y. A Comparative Study of Ultraviolet and Electron Beam Irradiation on Acrylate Coatings. *Egypt. J. Chem.* **2020**, *63*, 1931−1940.

(24) Li, S.; Wang, N.; Guo, J.; Zan, J.; Gao, Y.; Huang, S.; Du, B. Effect of electron beam irradiation on trap distribution of thermally aged PET film. *International Conference on High Voltage Engineering and Applications*; IEEE, 2016; pp. 1−4.

(25) Wasyluk, J.; Adley, D.; Perova, T. S.; Rodin, A. M.; Callaghan, J.; Brennan, N. Micro-Raman investigation of stress distribution in laser drilled via structures. *Appl. Surf. Sci.* **2009**, *255*, 5546−5548.
(26) Xu, Z.; He, Z.; Song, Y.; Fu, X.; Rommel, M.; Luo, X.; Hartmaier, A.; Zhang, J.; Fang, F. Topic Review: Application of Raman Spectroscopy Characterization in Micro/Nano-Machining. *Micromachines* **2018**, *9*, 361.
(27) Lam, J. C. K.; Huang, M. Y. M.; Hau Ng, T.; Khalid Bin Dawood, M.; Zhang, F.; Du, A.; Sun, H.; Shen, Z.; Mai, Z. Evidence of ultra-low-k dielectric material degradation and nanostructure alteration of the Cu/ultra-low-k interconnects in time-dependent dielectric breakdown failure. *Appl. Phys. Lett.* **2013**, *102*, 022908.
(28) Liu, Z.; Luo, N.; Shi, J.; Zhang, Y.; Xie, C.; Zhang, W.; Wang, H.; He, X.; Chen, Z. Raman spectroscopy for the discrimination and quantification of fuel blends. *J. Raman Spectrosc.* **2019**, *50*, 1008−1014.
(29) Dong, F.; Maganty, S.; Meschter, S. J.; Nozaki, S.; Ohshima, T.; Makino, T.; Cho, J. Electron beam irradiation effect on the mechanical properties of nanosilica-filled polyurethane films. *Polym. Degrad. Stab.* **2017**, *141*, 45−53.
(30) Song, M.-L.; Yu, H.-Y.; Chen, L.-M.; Zhu, J.-Y.; Wang, Y.-Y.; Yao, J.-M.; Zou, Z.; Tam, K. C. Multibranch Strategy To Decorate Carboxyl Groups on Cellulose Nanocrystals To Prepare Adsorbent/Flocculants and Pickering Emulsions. *ACS Sustainable Chem. Eng.* **2019**, *7*, 6969−6980.
(31) Thiha, A.; Ibrahim, F.; Muniandy, S.; Madou, M. J. Microplasma direct writing for site-selective surface functionalization of carbon microelectrodes. *Microsyst. Nanoeng.* **2019**, *5*, 62.
(32) Bayat, A.; Saievar-Iranizad, E. Vertically aligned rutile TiO2 nanorods sensitized with sulfur and nitrogen co-doped graphene quantum dots for water splitting: An energy level study. *J. Alloys Compd.* **2018**, *755*, 192−198.
(33) Faniyi, I. O.; Olofinjana, B.; Adekunle, A. S.; Oluwasusi, T. V.; Eleruja, M. A.; Ajayi, E. O. B. The comparative analyses of reduced graphene oxide (RGO) prepared via green, mild and chemical approaches. *SN Appl. Sci.* **2019**, *1*, 1181.
(34) Johnson, L. M.; Gao, L.; Shields IV, C.; Smith, M.; Efimenko, K.; Cushing, K.; Genzer, J.; López, G. P. Elastomeric microparticles for acoustic mediated bioseparations. *J. Nanobiotechnol.* **2013**, *11*, 22.
(35) Wang, C. Y.; Zheng, J. Z.; Shen, Z. X.; Lin, Y.; Wee, A. T. S. Elimination of O2 plasma damage of low-k methyl silsesquioxane film by As implantation. *Thin Solid Films* **2001**, *397*, 90−94.
(36) Jing, S. Y.; Lee, H.; Choi, C. Chemical bond structure on Si-O-C composite films with a low dielectric constant deposited by using inductively coupled plasma chemical vapor deposition. *J. Korean Phys. Soc.* **2002**, *41*, 769−773.
(37) Oh, T.; Choi, C. K. Comparison Between SiOC Thin Film by Plasma Enhance Chemical Vapor Deposition and SiO2 Thin Film by Fourier Transform Infrared Spectroscopy. *J. Korean Phys. Soc.* **2010**, *56*, 1150−1155.
(38) Grodzicki, M.; Wasielewski, R.; Surma, S. A.; Ciszewski, A. Formation of Excess Silicon on 6H-SiC(0001) during Hydrogen Etching. *Acta Phys. Pol., A* **2009**, *116*, S82−S85.
(39) Long, W.; Li, H.; Yang, B.; Huang, N.; Liu, L.; Gai, Z.; Jiang, X. Superhydrophobic diamond-coated Si nanowires for application of anti-biofouling'. *J. Mater. Sci. Technol.* **2020**, *48*, 1−8.
(40) Molina, C.; Dahmouche, K.; Hammer, P.; Bermudez, V. d. Z.; Carlos, L. D.; Ferrari, M.; Montagna, M.; Gonçalves, R. R.; Oliveira, L. F. C. d.; Edwards, H. G. M.; Messaddeq, Y.; Ribeiro, S. J. L. Structure and properties of Ti4+-ureasil organic-inorganic hybrids. *J. Braz. Chem. Soc.* **2006**, *17*, 443−452.
(41) Zhuo, Z.; Sannomiya, Y.; Kanetani, Y.; Yamada, T.; Ohmi, H.; Kakiuchi, H.; Yasutake, K. Interface properties of SiOxNy layer on Si prepared by atmospheric-pressure plasma oxidation-nitridation. *Nanoscale Res. Lett.* **2013**, *8*, 201.
(42) Coxon, P. R.; Coto, M.; Juzeliunas, E.; Fray, D. J. The use of electro-deoxidation in molten salts to reduce the energy consumption of solar grade silicon and increase the output of PV solar cells. *Prog. Nat. Sci.: Mater. Int.* **2015**, *25*, 583−590.
(43) Freund, H.-J.; Pacchioni, G. Oxide ultra-thin films on metals: new materials for the design of supported metal catalysts. *Chem. Soc. Rev.* **2008**, *37*, 2224−2242.
(44) Moniruzzaman, K. M. *Development of a single-step fabrication process for nanoimprint stamps*; Academic Press: Lund, 2011; p 31.
(45) Zatsepin, A. F.; Kuznetsova, Y. A.; Wong, C. H. Creation of Si quantum dots in a silica matrix due to conversion of radiation defects under pulsed ion-beam exposure. *Phys. Chem. Chem. Phys.* **2019**, *21*, 25467−25473.
(46) Lamastra, F. R.; Mori, S.; Cherubini, V.; Scarselli, M.; Nanni, F. A new green methodology for surface modification of diatomite filler in elastomers. *Mater. Chem. Phys.* **2017**, *194*, 253−260.
(47) Ma, J. W.; Lee, W. J.; Bae, J. M.; Jeong, K. S.; Oh, S. H.; Kim, J. H.; Kim, S.-H.; Seo, J.-H.; Ahn, J.-P.; Kim, H.; Cho, M.-H. Carrier Mobility Enhancement of Tensile Strained Si and SiGe Nanowires via Surface Defect Engineering. *Nano Lett.* **2015**, *15*, 7204−7210.
(48) Wan Isahak, W. N. R.; Manal, I.; Nordin, N. M.; Hamzah, N.; Ghoreishi, K. B.; Jahim, J. M.; Yarmo, M. A. Synthesis and Characterization of Silicotungstic Acid Nanoparticles via Sol Gel Technique as a Catalyst in Esterification Reaction. *Adv. Mater. Res.* **2011**, *364*, 266−271.
(49) Wu, Y.; Lin, Y.; Xu, J. Synthesis of Ag-Ho, Ag-Sm, Ag-Zn, Ag-Cu, Ag-Cs, Ag-Zr, Ag-Er, Ag-Y and Ag-Co metal organic nanoparticles for UV-Vis-NIR wide-range bio-tissue imaging. *Photochem. Photobiol. Sci.* **2019**, *18*, 1081−1091.
(50) Bazylewski, P.; Boukhvalov, D. W.; Kukharenko, A. I.; Kurmaev, E. Z.; Hunt, A.; Moewes, A.; Lee, Y. H.; Cholakh, S. O.; Chang, G. S. The characterization of Co-nanoparticles supported on graphene. *RSC Adv.* **2015**, *5*, 75600−75606.
(51) Yang, D.; Velamakanni, A.; Bozoklu, G.; Park, S.; Stoller, M.; Piner, R. D.; Stankovich, S.; Jung, I.; Field, D. A.; Ventrice, C. A.; Ruoff, R. S., Jr Chemical analysis of graphene oxide films after heat and chemical treatments by X-ray photoelectron and Micro-Raman spectroscopy. *Carbon* **2009**, *47*, 145−152.
(52) Sadri, R.; Hosseini, M.; Kazi, S. N.; Bagheri, S.; Zubir, N.; Solangi, K. H.; Zaharinie, T.; Badarudin, A. A bio-based, facile approach for the preparation of covalently functionalized carbon nanotubes aqueous suspensions and their potential as heat transfer fluids. *J. Colloid Interface Sci.* **2017**, *504*, 115−123.

https://doi.org/10.1021/acsomega.1c01429
ACS Omega 2021, 6, 13384−13390